Icarus 425 (2025) 116319

Contents lists available at ScienceDirect

Icarus

journal homepage: www.elsevier.com/locate/icarus

Research Paper

The direction of core solidification in asteroids: Implications for dynamo generation

K.H. Dodds [a,*], J.F.J. Bryson [b], J.A. Neufeld [a,c,d], R.J. Harrison [a]

[a] Department of Earth Sciences, University of Cambridge, Downing Street, Cambridge, CB2 3EQ, UK
[b] Department of Earth Sciences, University of Oxford, South Parks Road, Oxford, OX1 3AN, UK
[c] Department of Applied Mathematics and Theoretical Physics, University of Cambridge, Centre for Mathematical Sciences, Wilberforce Road, Cambridge, CB3 0WA, UK
[d] Institute for Energy and Environmental Flows, University of Cambridge, Madingley Road, Cambridge, CB3 0EZ, UK

ARTICLE INFO

Keywords:
Asteroids
Magnetic fields

ABSTRACT

Paleomagnetic studies of meteorites over the past two decades have revealed that the cores of multiple meteorite parent bodies, including those of certain chondritic groups, generated dynamo fields as they crystallised. However, uncertainties in the direction and mode of core solidification in asteroid-sized bodies have meant using the timings and durations of these fields to constrain parent body properties, such as size, is challenging. Here, we use updated equations of state and liquidus relationships for Fe-FeS liquids at low pressures to calculate the locations at which solids form in these cores. We perform these calculations for core-mantle boundary (CMB) pressures from 0–2 GPa, and Fe-FeS liquid concentrations on the iron-rich side of the eutectic, as well as two values of iron thermal expansivity that cover the measured uncertainties in this parameter, and adiabatic and conductive cooling of these cores. We predict inward core crystallisation from the CMB in asteroids due to their low < 0.5 GPa pressures regardless of the uncertainties in other key core parameters. However, due to low internal pressures in these cores, remelting of any iron snow, as proposed to generate Ganymede's present-day field, may be unlikely as the cores are approximately isothermal. Therefore a different mode of inward core solidification is possibly required to explain compositionally-driven dynamo action in asteroids. Additionally, we identify possible regimes at higher $> 0.6 - 2$ GPa pressures in which crystallisation can occur concurrently at the CMB and the centre.

1. Introduction

The crystallisation of a liquid iron alloy core can be a highly efficient process for generating a self-exciting dynamo (Nimmo, 2009, Nimmo, 2015) because it can produce large (> 1000 kg m^{-3}) density differences and hence buoyancy forces that power convection. For instance, core crystallisation is responsible for the present-day dynamo activity and associated magnetic fields of Earth, Ganymede (Rückriemen et al., 2015) and Mercury (Breuer et al., 2007), as well as potentially for the ancient Moon (Weiss and Tikoo, 2014). Moreover, this process has been proposed to have powered the later periods of dynamo generation in asteroids during the first few hundred millions of years after the start of the solar system (Shah et al., 2017, Maurel et al., 2018, Bryson et al., 2019a, Maurel et al., 2020, Nichols et al., 2021). These rocky worlds span a large range of sizes, from < 100 km radii asteroids, to the Earth whose mean radius is 6731 km, and have experienced accretionary and differentiation histories of varying complexity. These differences have led to varying thermochemical structures within their cores (e.g. Stevenson et al., 1983, Driscoll and Bercovici, 2014), which introduce multiple potential mechanisms for dynamo activity throughout their lifetimes, culminating in the solidification of their cores.

The location at which a planetary body's core starts to solidify depends on the relationship between its temperature profile and its liquidus as well as the degree of supercooling required for nucleation. Recent studies have suggested a critical supercooling of > 600–1000 K is required for inner core nucleation under Earth-like conditions (Huguet et al., 2018, Sun et al., 2022, Wilson et al., 2023) and > 80 K for small planetary cores (Huguet et al., 2018). However in this study, we will determine the location of crystallisation in a planetary core as where its temperature profile first crosses its liquidus (Fig. 1) for simplicity.

* Correspondence to: LGL-TPE, École Normale Supérieure de Lyon, 46 Allée d'Italie, Lyon, 69007, France.
E-mail address: kathryn.dodds@ens-lyon.fr (K.H. Dodds).

https://doi.org/10.1016/j.icarus.2024.116319
Received 17 June 2024; Received in revised form 1 September 2024; Accepted 16 September 2024
Available online 19 September 2024

For the Earth (Fig. 1a), the high pressures within the core (> 135 GPa) lead to liquidus temperatures that increase more rapidly with depth than the adiabatic temperature, since it becomes increasingly favourable for iron to exist as a solid rather than a liquid at higher pressures and hence greater depths. Therefore, the Earth's core first cooled below the liquidus at its centre, nucleating an inner core and subsequently generating a dynamo field driven by outwards core crystallisation.

However, the other rocky bodies that are known to have, or previously had, a dynamo are far smaller than the Earth and thus their core pressures are lower, e.g. < 10 GPa for the Moon and Ganymede. This can result in a core liquidus that increases more slowly with depth within the core than the adiabat, causing the first solids to form at the CMB (Fig. 1b). Multiple dynamo mechanisms have been proposed for inwardly crystallising cores, such as the iron snow model for Ganymede, where iron crystals form at the CMB and sink into the hotter interior. The crystals then remelt, increasing the liquid density and driving convection and a dynamo (Rückriemen et al., 2015). Models of dynamo generation during top-down crystallisation in asteroids, e.g. Scheinberg et al. (2016) and Neufeld et al. (2019), have considered delamination of large metre-scale dendrites that stir up the core liquid sufficiently to generate a dynamo as they sink. However, these models have predominantly been developed to explain the magnetisation of the IVA iron meteorites and their unmantled parent body, and therefore may not be applicable to typical mantled asteroids.

The direction of core solidification is a key factor controlling the mechanisms by which planets and planetesimals are able to generate dynamos. However, the core crystallisation regime in which the cores of meteorite parent bodies lie is uncertain. Both Haack and Scott (1992) and Chabot and Haack (2006) invoke inward core crystallisation to explain the fractional crystallisation patterns observed in iron meteorites. The calculations from Haack and Scott (1992), which Chabot and Haack (2006) use to inform their prediction of the direction of crystallisation, are limited to pure iron cores because the equations of state and the liquidus behaviour of liquid iron alloys were not available at the time. More recently, Williams (2009) calculated the likely crystallisation regime for small solar system objects such as Ganymede and the Moon for a limited range of core sulfur contents (0, 5, 10 wt% S) based on the relative slopes of the liquidus and adiabat. That study concluded that asteroid cores with pressures < 2 GPa may crystallise either inwardly or outwardly, depending critically on the core's thermal expansivity, α, and sulfur composition.

Since the publication of Williams (2009), updated formulations of both the liquidus behaviour and equations of state of Fe-FeS alloys at low pressure have been published (Buono and Walker, 2011, and Rivoldini et al., 2009 and Morard et al., 2018, respectively), which allow for the consideration of a far wider range of core sulfur compositions than was possible by Williams (2009). Additionally, thermal evolution models of asteroids have shown that the CMB heat flux prior to the onset of core solidification may be either sub- or super-adiabatic, depending on core size and sulfur content (Bryson et al., 2019b), whereas Williams (2009) considered only adiabatic heat fluxes. A sub-adiabatic CMB heat flux would lead to a conductive temperature profile within the core with a lower temperature gradient compared to a convecting core, which may then affect its direction of solidification.

In this study, we determine the likely direction of core solidification in asteroid-sized bodies over a wider parameter range than was previously possible, using updated liquidus relationships and equations of state for Fe-FeS alloys at low pressures (< 2 GPa). We then use our results to explore which dynamo mechanisms are likely to be applicable to asteroid-sized cores and discuss any outstanding issues in our understanding of compositional dynamo generation during core solidification for these small rocky bodies. We identify five possible modes of core solidification within this pressure and composition range. For asteroids (i.e., bodies < 600 km in total radius), we predict inward core solidification, regardless of core sulfur composition, in contrast to Williams (2009). For larger bodies, we predict core solidification modes in which crystallisation could occur simultaneously at the centre and the CMB. These modes are relevant to bodies with CMB pressures of > 0.6 GPa to > 2 GPa, depending critically on sulfur concentration.

2. Theory

The location at which a planet's core starts to solidify depends on the relationship between the thermal structure of the core and that of the liquidus, or more generally the structure of the phase diagram. Previous studies investigating the direction of crystallisation in asteroids (e.g. Williams, 2009) used the relative pressure differentials of the core adiabat and liquidus to determine the expected direction of core solidification. In this linear approximation, outward crystallisation is predicted when

$$\frac{\partial T_c}{\partial P} < \frac{\partial T_l}{\partial P}, \tag{1}$$

where $\partial T_c/\partial P$ and $\partial T_l/\partial P$ are the pressure differentials of the core temperature and liquidus, respectively, with pressure acting as a proxy for depth within the core. Inward crystallisation instead occurs when

$$\frac{\partial T_c}{\partial P} > \frac{\partial T_l}{\partial P}. \tag{2}$$

However, this approach may not reveal all the different ways that small planetary cores can solidify because Buono and Walker (2011) found that the liquidus temperature of Fe-FeS liquids first decreases with pressure for all sulfur contents on the iron-rich side of the eutectic (< 32 wt% S) before it starts to increase at pressures of 0.75–1.50 GPa (Fig. 2). This minimum in the Fe-FeS liquidus at low pressures could lead to simultaneous solidification at multiple locations within a small planetary core, which in turn would affect the possible available dynamo driving mechanisms as well as the core's thermochemical evolution. Since evaluating only the pressure differentials of the core temperature and liquidus does not allow us to determine if a core could crystallise in more than one location contemporaneously, we instead calculate the temperature and liquidus as a function of pressure within small planetary cores. In general, the core temperature as a function of pressure is given by

$$T_c(P) = T_{CMB} + \int_{P_{CMB}}^{P} \frac{\partial T_c}{\partial P'} dP', \tag{3}$$

where T_{CMB} and P_{CMB} are the CMB temperature and pressure respectively, P' is a dummy variable, and $\partial T/\partial P'$ is the pressure differential of the core temperature, which depends not only on its sulfur concentration and pressure but also on the mechanism of heat transfer in the core at the onset of solidification, for which both convection and diffusion may have occurred. To calculate the temperature profile, we use a first-order Taylor expansion such that

$$T_c(P + \Delta P) = T_c(P) + \left.\frac{\partial T_c(P)}{\partial P}\right|_P \Delta P, \tag{4}$$

starting from the CMB, at which we set an initial CMB temperature such that all depths within the core are initially fully molten.

To determine where core crystallisation occurs, we first calculate the liquidus profile within a core of a given CMB pressure (Section 2.1). We then lower the CMB temperature incrementally, recalculating the temperature profile at each iteration (Section 2.2) to mimic core cooling. For simplicity, we neglect here both the effect of the release of latent heat during crystallisation as well as any chemical evolution of the core liquid on the temperature profile. We anticipate that the inclusion of latent heat and chemical evolution may alter the time dependence of cooling, but will not significantly alter the location or mode of early crystallisation. At each temperature step, we identify any pressures at which the core temperature is below the liquidus and thus crystallising. We continue lowering the CMB temperature until the entire core is below the liquidus. This approach allows us to

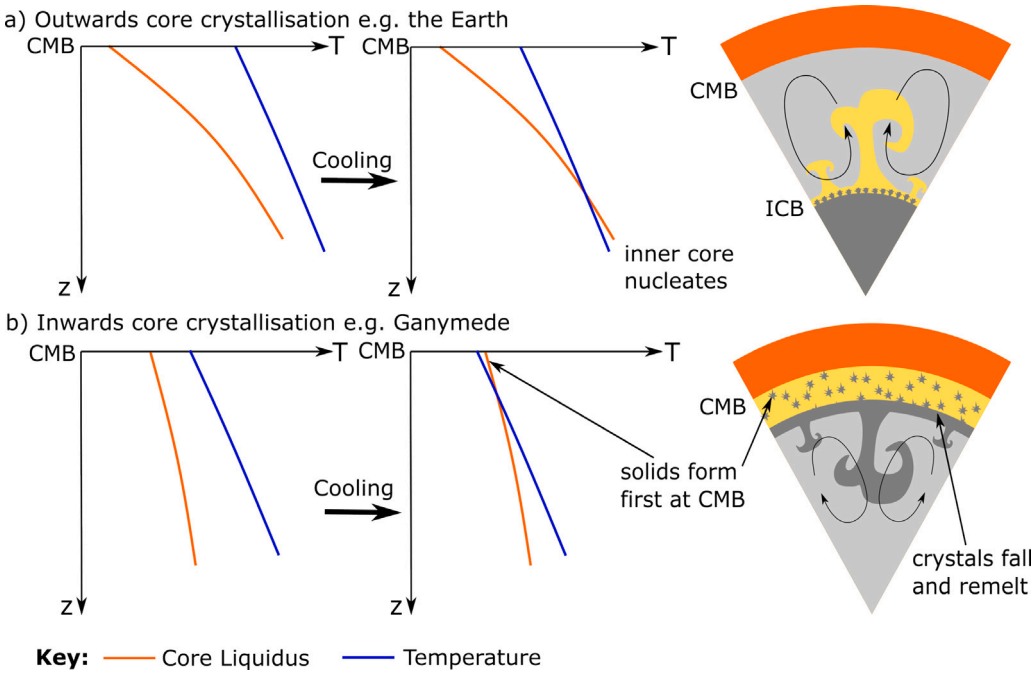

Fig. 1. Schematics of core crystallisation starting from (a) the centre of a planet's core, e.g. the Earth and (b) from below its core-mantle boundary e.g. Ganymede. The location at which the first solids form is governed by where the core's temperature profile first crosses its liquidus on cooling. This is controlled by the relative slopes of the core liquidus (orange line) and temperature (blue line). The temperature profile in a convecting core lies along an adiabat except within a narrow thermal boundary layer below the CMB (black dashed line). However this thermal boundary layer is not shown here as it is negligible. The direction of core crystallisation then controls the mechanism of dynamo generation. In outwardly crystallising cores, e.g. Earth, light-element enriched liquid is expelled from the inner core and rises buoyantly, mixing and driving convection (Loper, 1978). Dynamo generation in top-down crystallising cores is less well understood but Ganymede's dynamo has been proposed to be driven by the remelting of iron crystals that form at the CMB in its deep interior (Rückriemen et al., 2015). (For interpretation of the references to colour in this figure legend, the reader is referred to the web version of this article.)

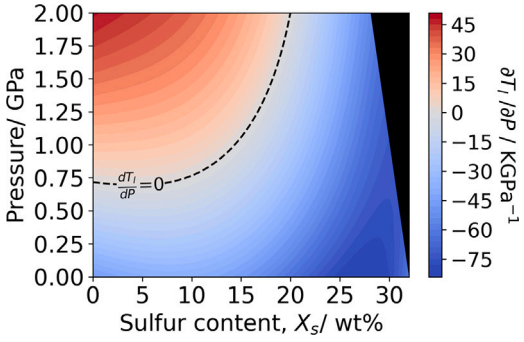

Fig. 2. Pressure derivative of the Fe-FeS Liquidus as a function of pressure and sulfur content for cores of < 5 GPa (Buono and Walker, 2011). The dashed line separates the high pressure regime (red), where the liquidus temperature increases with pressure, from the low pressure regime (blue) where the liquidus temperature decreases with pressure. The sulfur content of the Fe-FeS eutectic decreases with pressure; the black shaded region at high pressures and high sulfur contents represents super-eutectic Fe-FeS liquids for which the equations of state and liquidus behaviour used here are not valid. In the low pressure regime, regardless of the pressure dependence of the core adiabat, which is always positive, core crystallisation proceeds inwardly from the CMB. In the high pressure regime, both inward and outward core crystallisation are possible. The mode of solidification that operates depends on the pressure dependence of the core adiabat. Finally, for cores with pressures that span the minimum in the liquidus temperature (black dashed line), crystallisation may occur simultaneously at multiple locations. (For interpretation of the references to colour in this figure legend, the reader is referred to the web version of this article.)

investigate the potential evolution of core crystallisation as well as its initial location and direction.

In the following sections, we detail the Fe-FeS liquidus surface and equation of state required to calculate the core temperature and liquidus as a function of pressure, and so determine the possible regimes in which asteroid cores crystallise. We vary P_{CMB} between 0–2 GPa, which corresponds to the expected CMB pressures of fully differentiated asteroids that have not undergone any sufficient mantle stripping during impacts with cores of radii $\leq$ 600 km, assuming a core/planetary radius ratio, Rc/Rp = 0.5.

We also consider both adiabatic and sub-adiabatic CMB heat fluxes, as previous models of asteroid thermal evolution predict that these cores cooled conductively for much of their history (Bryson et al., 2019b), including prior to core solidification. Additionally we consider two values for the thermal expansivity of liquid iron, 9.2×10^{-5} K^{-1} and 1.32×10^{-4} K^{-1} (Williams, 2009), and core sulfur contents of $\leq$ 32 wt% S as these two quantities carry large uncertainties due to difficulties associated with measuring them accurately.

2.1. Pressure dependence of the core liquidus

Based on a compilation of experimental Fe-FeS melting studies at 1 bar, 3 GPa, 6 GPa and 10 GPa, Buono and Walker (2011) give the pressure and sulfur concentration dependence of the Fe-FeS liquidus as

$$T_l(X_{mol}^{FeS}, P) = A(P)(X_{mol}^{FeS})^4 + B(P)(X_{mol}^{FeS})^3 + C(P)(X_{mol}^{FeS})^2 + D(P)(X_{mol}^{FeS}) + E(P), \quad (5)$$

where X_{mol}^{FeS} is the molar content of FeS in the core, P is the pressure in GPa and A, B, C, D and E are pressure-dependent constants. The values of these constants are approximately given by

$$\begin{aligned} A(P) &= -2.4724P^4 + 28.025P^3 + 9.1404P^2 + 581.71P + 3394.8, \\ B(P) &= 1.7978P^4 - 6.7881P^3 - 197.69P^2 - 271.69P - 8219.5, \\ C(P) &= 0.1702P^4 - 9.3959P^3 + 163.53P^2 - 319.35P + 5698.6, \\ D(P) &= 0.2308P^4 + 7.1P^3 - 64.118P^2 + 105.98P - 1621.9, \\ E(P) &= 0.2302P^4 - 5.3688P^3 + 38.124P^2 - 46.681P + 1813.8. \end{aligned} \quad (6)$$

This formulation for the Fe-FeS liquidus is valid for pressures < 10 GPa, i.e. for bodies of Ganymede's size or less, and sulfur contents on the iron-rich side of the eutectic, with a goodness of fit to their experimental results of R^2 = 0.901 for 1 bar, R^2 = 0.996 for 3 GPa, R^2 = 0.970 for 6 GPa, and R^2 = 0.998 for 10 GPa (Buono and Walker, 2011). We have chosen to use this model instead of others such as Dorogokupets et al. (2017) or Liu and Li (2020) as it covers the entire pressure and sulfur concentration range in which planetesimal bodies lie. Therefore, it is worth noting that our predicted core crystallisation regimes will depend on this choice of liquidus model.

2.2. Pressure dependence of the core temperature

Models of asteroid thermal evolution, for example by Bryson et al. (2019b), have shown that asteroid cores likely cooled by conduction prior to core solidification as heat loss out of their silicate mantles at that time was low (< 10 mW m^{-2}). Conductive cooling results in a core temperature profile that increases less rapidly with depth and pressure compared to convective cooling, thereby this initial core condition possibly promotes outwards core solidification.

However, these models of asteroid evolution generally consider cores with a eutectic sulfur concentration which start to crystallise at 1234 K. This low liquidus temperature leads to core crystallisation occurring late, long after magma ocean convection ceases, when the body is cooling slowly. From the iron meteorite record, the inferred sulfur content of asteroid cores is 0 – 14 wt% S (Goldstein et al., 2009). For such low < 14 wt% S cores, we would expect core crystallisation to begin earlier, i.e. during the period of magma ocean convection when the CMB heat flux is superadiabatic due to higher > 1550 K CMB liquidus temperatures (Bryson et al., 2019b) predicted for low pressure (< 1 GPa) cores. However, many of the lowest sulfur iron meteorite groups show evidence for impact-driven volatile loss (Goldstein et al., 2009). Therefore these low inferred sulfur contents may not represent the original core composition. Nonetheless, it is worth considering low core sulfur concentrations as they could result in cores that convect prior to the onset of core solidification, and hence possibly favour inwards core solidification.

Given this dependence on sulfur content for the initial core temperature profile, we therefore calculate the expected regime of core solidification for both super- and sub-adiabatic CMB heat fluxes to explore the full effect of CMB heat flux on core crystallisation.

2.2.1. In a convecting core

If a core is convecting, its thermal profile lies along the core adiabat except in a narrow thermal boundary layer below the CMB. However, given the low viscosity of the core liquid, both the thickness and temperature difference across this boundary layer is negligible so we do not include it in our core temperature profile. In asteroid-sized bodies, core convection requires heat fluxes out of the CMB of approximately 10 mW m^{-2} (Bryson et al., 2019b). Following Williams (2009), the pressure differential of the adiabatic temperature, T_{ad}, of the core is given by

$$\frac{\partial T_{ad}}{\partial P} = \frac{1}{\rho g(r)} \frac{\partial T_{ad}}{\partial r} = \frac{\alpha T_{ad}}{\rho c_p}, \quad P_{CMB} < P < P_c \tag{7}$$

where α, ρ and c_p are the core thermal expansivity, density and specific heat capacity, respectively, and P_c is the pressure at the centre of the core. These parameters are all functions of the core pressure, temperature, and light element concentration. For the core light element concentration, we consider only variations in the sulfur content of these cores, X_s, since sulfur has a large effect on the core liquidus (Buono and Walker, 2011), as well as density and thermal parameters such as c_p (Kanda et al., 1986).

We take the specific heat capacity to be only a function of sulfur content over the pressure–temperature range considered here. Following Williams (2009) and Morard et al. (2018), this is given by linear interpolation between its value for pure iron, $c_{p,Fe}$ = 850 J kg^{-1} K^{-1} (Elkins-Tanton et al., 2011), and its value for pure FeS, $c_{p,FeS}$ = 454 J kg^{-1} K^{-1} (Kanda et al., 1986).

To calculate the density of the Fe-FeS liquid as a function of pressure, sulfur content and temperature, we follow Morard et al. (2018), who provide an equation of state for these liquids for P < 5 GPa, T < 1900 K, and X_s < 32 wt% S, i.e., the parameter space in which asteroid cores exist. The pressure dependence of the liquid density is described by a third-order Birch–Murnaghan equation (Morard et al., 2018), where

$$P = \frac{3}{2} K_{T,0} \left[f^{7/3} - f^{5/3}\right] \left[1 + \frac{3}{4}\left(K'_{T,0} - 4\right)\right] \left(f^{2/3}\right) - 1. \tag{8}$$

Here we define

$$f = \frac{\rho_P}{\rho_0}, \tag{9}$$

where ρ_P is the density at the required pressure and sulfur content, ρ_0, is the reference density of a liquid with the same sulfur content at the reference pressure of P = 1 bar, and both are at a reference temperature of T_0 = 1900 K. $K_{T,0}$ is the isothermal bulk modulus of the liquid Fe-FeS evaluated at the liquidus temperature and P = 0 GPa, and $K'_{T,0}$ is the first derivative of this modulus with respect to pressure, also evaluated at the same reference conditions. The reference density as a function of sulfur content is given by

$$\rho_0 = -3108 \left(X^S_{mol}\right)^2 - 5176 X^S_{mol} + 6950 \tag{10}$$

in kg m^{-3} where X^S_{mol} is the core molar sulfur content (Morard et al., 2018). The isothermal bulk modulus at ambient pressure as a function of molar sulfur content is given by

$$K_{T,0} = \left(K_{T,Fe}\right)^{1-X^S_{mol}} \times \left(K_{T,S}\right)^{X^S_{mol}}, \tag{11}$$

where $K_{T,Fe}$ = 76 GPa and $K_{T,S}$ = 1.6 GPa. While linear mixing models are often used for bulk moduli, as in Rivoldini et al. (2009), these are only valid for small compositional ranges. In previous studies, Morard et al. (2013) and Morard et al. (2018) find this form more suitable for the large compositional range considered in their experiments. The pressure derivative of the bulk modulus as a function of molar sulfur content is given by

$$K'_{T,0} = K'_{Fe} + 3X^S_{mol}, \tag{12}$$

where K'_{Fe} = 6.5 (Morard et al., 2018). Combining Eqs. (8) and (10) allows us to calculate the liquid density, $\rho(T_0, P, X_S)$, as a function of pressure and sulfur content at T_0 = 1900 K. For the temperature variation of the density, we assume a linear dependence of density on temperature, following Morard et al. (2018) and Williams (2009). This has been shown to be a valid approximation for Fe liquids by Assael et al. (2006) for T < 2500 K. As such, the density of an Fe-FeS liquid as a function of pressure, temperature and sulfur content is given by

$$\rho(T, P, X_s) = \rho(T_0, P, X_s)\left[1 + \alpha(T_0 - T)\right]. \tag{13}$$

Finally, the thermal expansivity of core liquid at a given pressure and temperature is calculated by

$$\alpha(P, T) = \frac{\alpha_0 K_{T,0}}{K_T(P, T)}, \tag{14}$$

where $K_T(P, T)$ is the isothermal bulk modulus of the liquid and $K_{T,0}$ and α_0 are the isothermal bulk modulus and thermal expansivity at the reference conditions of P = 0 GPa and T, the current core temperature. While this reference thermal expansivity is technically a function of both temperature and sulfur concentrations, we assume here that it is constant over the temperature range we are considering as its value has been shown to be constant for liquid iron at temperatures T < 2500 K (Assael et al., 2006). Additionally, we assume this parameter is constant for all sulfur concentrations as it is not well constrained for pure liquid iron at low pressures, let alone for intermediate sulfur concentrations (Williams, 2009, Morard et al., 2018, Xu et al., 2021).

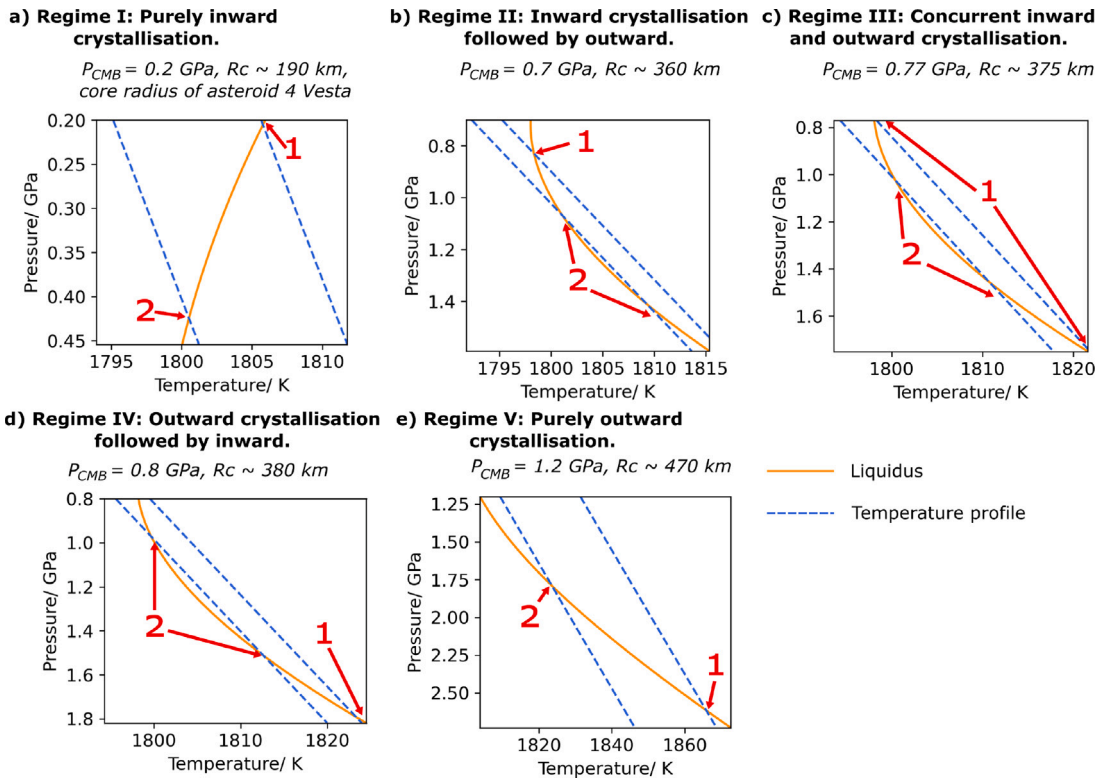

Fig. 3. Examples of the different predicted regimes of core crystallisation in small planetary cores. For all five examples shown here, the core liquid is pure iron and it is convecting thus the temperature profiles (blue dashed lines) represent the core adiabat, calculated here with $\alpha_{Fe} = 9.2 \times 10^{-5}$ K^{-1}. We consider the core to be solidifying at pressures where the core adiabat is cooler than the liquidus (solid orange line). The crystallisation sequence is denoted by the red numbers and the locations of crystallisation by the red arrows. Core cooling is approximated by gradually decreasing the CMB temperature, and maintaining a purely adiabatic temperature profile. We find these five regimes are present for all considered sulfur contents and both convecting and conducting cores as their existence is a product of the low pressure liquidus behaviour observed in Fe-FeS liquids. However, the intermediate regimes (II to IV) are restricted to small pressure ranges in conducting cores due to the small temperature gradient in these cores. (For interpretation of the references to colour in this figure legend, the reader is referred to the web version of this article.)

Therefore we adopt two values: a high value of $\alpha_0 = 1.3 \times 10^{-4}$ K^{-1} (Assael et al., 2006) and a low value of $\alpha_0 = 9.2 \times 10^{-5}$ K^{-1} (Hauck et al., 2006). These two values cover the range of measured iron and Fe-S thermal expansivities (Williams, 2009) and reflect the uncertainty in this key parameter.

2.2.2. In a conducting core

If the CMB heat flux is subadiabatic (< 10 mW m^{-2}), the core will cool conductively across its entire depth. In this case, the temperature will increase less rapidly with depth when compared to the convecting, adiabatic regime. In order to calculate the temperature profile within a conducting core, we assume that the core is in thermal equilibrium, i.e., its temperature profile is well-approximated by the equilibrium steady state profile. This enables us to calculate the temperature profile, given an imposed heat flux out of the CMB. The pressure differential of this conductive temperature profile can then be written as

$$\frac{\partial T_c}{\partial P} = -\frac{F_{CMB}}{k_c}\left(\frac{\partial P}{\partial r}\right)^{-1}, \tag{15}$$

where F_{CMB} is the CMB heat flux, k_c is the core thermal conductivity, and $\partial P/\partial r$ is the pressure gradient in the core, which is taken to be hydrostatic. Therefore Eq. (15) becomes

$$\frac{\partial T_c}{\partial P} = \frac{F_{CMB}}{k_c}\frac{1}{\rho(T, P, X_s)g}, \tag{16}$$

where the density of the core liquid is calculated by Eqs. (8) through (14) and g is the gravitational acceleration at the CMB. Here we consider a sub-adiabatic heat flux of 1 mW m^{-2}, and $k_c = 30$ W m^{-1} K^{-1} (Opeil SJ et al., 2012) which we assume to be constant over the pressure range < 2 GPa, to explore the effect this has on the expected direction of core solidification in asteroids. However, the quantity F_{cmb}/k_c is a free parameter due to the large uncertainties in the core thermal conductivity (Manthilake et al., 2019), and the time evolution of the CMB heat flux during core crystallisation.

3. Results

In this section, we present the possible regimes (Fig. 3) and regime maps for the expected direction of core solidification in asteroids (Fig. 4) covering a core pressure range of < 2 GPa and sulfur contents of ≤ 32 wt% S. We predict five different crystallising regimes for small planetary cores (Fig. 3) depending on where the first solids form, and then, by any other potential locations of core freezing. These five regimes are defined as following: Regime I, purely inwards crystallisation; Regime II, initially inwards crystallisation followed by outwards crystallisation; Regime III, in which crystallisation starts concurrently at the CMB and at the centre; Regime IV, initially outwards crystallisation followed by inwards crystallisation; and Regime V, purely outwards crystallisation.

We find that Regime I, in which solidification first occurs at the CMB and proceeds inwardly for the entirety of core crystallisation (Fig. 3a), is the dominant mode of solidification for both convecting and conducting cores, especially those with high > 10 wt% S contents and for the high thermal expansivity value of $\alpha_{Fe} = 13.2 \times 10^{-5}$ K^{-1}. The maximum permitted CMB pressure for a low sulfur concentration, < 10 wt% S, convecting core to undergo purely inwards core crystallisation is 0.6 GPa and 0.7 GPa for the low and high values of thermal expansivity, respectively (Fig. 4a–b). For higher ~ 20 wt% sulfur concentration, convecting cores, purely inwards core crystallisation is expected up to CMB pressures > 2.0 GPa for both the high and low values of α_{Fe}. In a conducting core (Figs. 4c–d), purely inward core crystallisation

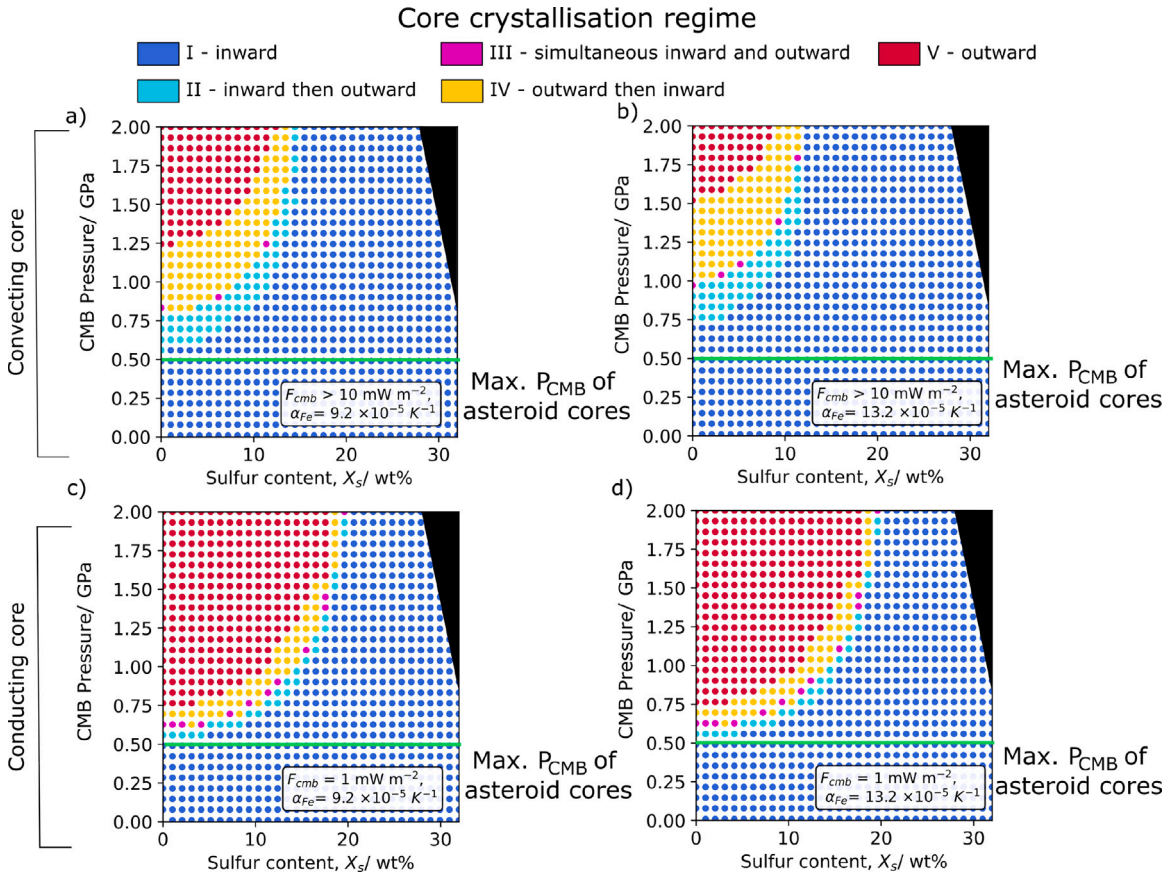

Fig. 4. Expected directions of core solidification as a function of CMB pressure, core sulfur content, CMB heat flux and the thermal expansivity of liquid iron. The regimes are defined in Fig. 3. The black shaded region indicates super-eutectic Fe-FeS liquids for which the liquidus surface given in Buono and Walker (2011) is no longer valid. The maximum expected P_{CMB} for asteroids is ~ 0.5 GPa, which could correspond to an asteroid with a core radius of ~ 300 km and total radius of ~ 600 km.

occurs at pressures up to ~ 0.5 GPa for low sulfur concentration cores, and pressures of > 2.0 GPa for high sulfur concentration cores. These lower pressures are permitted as the temperature gradient within the core is lower for a conducting core compared to a convecting one. Regardless, for asteroid-like CMB pressures ≤ 0.5 GPa, corresponding to a 300 km radius core under a 300 km thick mantle, we predict that core crystallisation will proceed from the CMB towards the centre for the entirety of core solidification. This is because the pressure differential of the Fe-FeS liquidus being negative, that is the liquidus temperature decreases with depth in these cores (Fig. 2), and this result is independent of sulfur concentration or the mode of heat transfer within the core at onset time of core solidification.

In Regime II, the core first crystallises at the CMB, and then after continued cooling, also nucleates an inner core while still freezing in a layer at the top of the core (Fig. 3b). This is possible due to the pressure differential of the liquidus changing from negative, (i.e. the liquidus decreasing with depth in the core), to positive, (i.e. the liquidus starts to increase with depth at intermediate pressures (0.75–1.4 GPa, depending on sulfur content)). As a result, after sufficient core cooling, the core temperature profile, which always increases with depth, can intersect the liquidus profile both at the top of the core and at the centre. This regime is limited to pressures of 0.6–0.8 GPa (R_c ~ 350–370 km) and 0.8–1.0 GPa (R_c ~ 380–420 km) for a pure iron, convecting core with the low and high values of α_{Fe}, respectively. For higher sulfur concentration (> 15 wt% S) and for convecting cores, we do not observe this regime as the pressure differential of the liquidus is negative in this region of parameter space. In a conducting core, this regime is confined to a narrow range of pressures ~ 0.1 GPa higher than the maximum permitted for Regime I for low (< 18 wt% S) sulfur cores. This is due to the small temperature gradient within these cores, which reduces the likelihood of the temperature profile crossing the liquidus profile more than once.

For very specific combinations of P_{CMB} and X_s, we find that core crystallisation starts concurrently at the CMB and at the centre of these cores (Regime III, Fig. 3c). This is only possible when the overall temperature difference across the core is equal to the overall difference in liquidus temperature between the CMB and the centre. Therefore, this regime occurs at the highest pressures for convecting cores with $\alpha_{Fe} = 13.2 \times 10^{-5}$ K^{-1} (Fig. 4a) and the lowest pressures for conducting cores (Figs. 4c–d) as these cores have the greatest and smallest core temperature gradients, respectively.

Cores in regime IV on the other hand are predicted to first nucleate an inner core and then, after further cooling, start to crystallise at the CMB as well (Fig. 3d). This regime only occurs for pressures greater than those that define the minimum in the liquidus surface, i.e. pressures over which the liquidus always increases with depth. At these pressures, the liquidus temperature increases more rapidly with increasing pressure ($\partial^2 T_l / \partial P^2 > 0$). This results in a concave-up liquidus profile across these cores compared to the (approximately) linear temperature profile. Therefore, it is possible for the temperature profile to intersect the liquidus near the top of the core, as well as at the bottom, and thus for the core to simultaneously crystallise inwardly from the CMB as well as grow an inner core. Regime IV occurs over a wide parameter range in convecting cores for sulfur contents < 15 wt% S and pressures from 0.8 GPa up to > 2 GPa (R_c ~ 380 – > 600 km) for $\alpha_{Fe} = 9.2 \times 10^{-5}$ K^{-1}, and for sulfur contents < 13 wt% S and pressures from 1.0 GPa up to > 2 GPa (R_c ~ 410 – > 600 km) for $\alpha_{Fe} = 13.2 \times 10^{-5}$ K^{-1}. However in conducting cores, this regime is restricted to a narrower range of permitted pressures. For a low sulfur concentration , conducting core, it can occur over a small ~ 0.1 GPa

pressure range, for example with X_s = 10 wt% S, the pressure range is 0.8–0.9 GPa (R_c ~ 380–400 km). For higher values of core sulfur content, such as X_s = 18 wt% S, regime IV can occur over a wider pressure range from 1.6 – > 2.0 GPa (R_c ~ 530 – > 600 km).

Finally, it is only possible for low sulfur concentration, high pressure cores to crystallise outwardly throughout their entire solidification (Regime V, Fig. 3e). In convecting cores, sulfur contents < 13 wt% S and pressures > 1.2 GPa (R_c > 500 km) are required for $\alpha_{Fe} = 9.2 \times 10^{-5}$ K^{-1}, in order for core crystallisation to be completely outward. For the higher value of $\alpha_{Fe} = 13.2 \times 10^{-5}$ K^{-1}, sulfur contents < 8 wt% S and pressures > 1.5 GPa (R_c > 510 km) are instead required. If the core is conducting at the start of core crystallisation, purely outwards core solidification is possible at lower pressures due to the smaller temperature gradient within these cores. For a low sulfur core, this could occur in cores with P_{CMB} > 0.8 GPa, for example in a core radius of 360 km, whereas in high sulfur cores, this requires pressures > 1.5 GPa, corresponding to cores with radii > 510 km.

4. Discussion

4.1. Comparison to previous studies

Our results show that inward core solidification is the dominant direction in cores with CMB pressures < 0.5 GPa, regardless of sulfur concentration or mode of heat transfer. By contrast, outwards core solidification is restricted to large, low sulfur cores. For a convecting core, the minimum pressure required for core solidification to begin at the centre is 1.2 GPa and 1.5 GPa for high and low thermal expansivities, respectively, and these minimum pressures require a pure iron core. Higher core sulfur contents raise the minimum pressure requirement further (Fig. 4) while lower sub-adiabatic heat fluxes allow for smaller, more sulfur-rich cores (Fig. 4c–d) initially to crystallise outwardly. However, even in the most favourable conditions (Regime V), the minimum pressure required for purely outwards crystallisation corresponds to a 360 km core radius, (i.e., > 720 km radius body). This would make such a body significantly larger than Ceres, the largest object in the asteroid belt at present-day with a radius of 473 km. Therefore we consider inward solidification to be the most likely direction of core crystallisation in the vast majority of asteroids, regardless of sulfur content or core thermal expansivity. This is in agreement with Haack and Scott (1992) and Chabot and Haack (2006), both of which predict inward core crystallisation for pure iron cores.

However, our results differ from those of Williams (2009) in which outwards core solidification is predicted for pure iron cores at all pressures when the lower bound of thermal expansivity $\alpha_{Fe} = 9.2 \times 10^{-5}$ K^{-1} is used. This difference stems from the descriptions of the pressure differential of the liquidus $\partial T_l/\partial P$ in the two studies. Williams (2009) adopts a constant value of $\partial T_l/\partial P \approx 35$ K GPa^{-1} from Strong et al. (1973), whereas we have adopted an updated liquidus relationship from Buono and Walker (2011) that covers a larger pressure and composition range than Strong et al. (1973). This updated liquidus relationship results in a liquidus slope that varies considerably with both these variables (Fig. 2). This includes a low pressure region ($P <$ 0.7 GPa) where $\partial T_l/\partial P < 0$ and thus inward solidification is expected for all sulfur contents. However, the behaviour of Fe-FeS liquidus is not well studied experimentally at pressures < 2 GPa, with more attention being targeted at the intermediate 5 – 10 GPa and high $P \gg$ 10 GPa pressures relevant to both Ganymede and the Moon, and the Earth's core, respectively (Morard et al., 2007 and Morard et al., 2014). Therefore, the true behaviour of the Fe-FeS liquidus for pressures relevant to asteroid-sized bodies is a key outstanding uncertainty in these thermodynamic calculations, and further refinement would allow for more accurate determination of the expected core crystallisation direction.

Williams (2009) also considers the effect of core sulfur content on the direction of core solidification. However, this previous study only considered values of 5 wt% S and 10 wt% S whereas we consider all compositions on the iron-rich side of the Fe-FeS eutectic. Inward crystallisation is predicted for 10 wt% S cores for P < 10 GPa regardless of the choice of α_{Fe}, and for 5 wt% S cores for $P <$ 10 GPa and $P <$ 4.5 GPa with $\alpha_{Fe} = 13.2 \times 10^{-5}$ K^{-1} and $\alpha_{Fe} = 9.2 \times 10^{-5}$ K^{-1}, respectively. Our study predicts that inward solidification will only occur at significantly lower pressures (< 0.8–1.2 GPa) than these for same sulfur concentrations (Figs. 4a–b). This difference is again due to the different liquidus maps used in each study and highlights the importance for better determining the Fe-FeS liquidus under asteroidal conditions. However, the pressures at which we predict outwards core solidification in convecting low S cores are still greater than those expected in asteroid-size cores. Therefore we still expect inwards to be the dominant solidification direction in asteroid cores. Additionally, our results indicate that for a given pressure and core size, the addition of sulfur promotes inward core solidification, in agreement with the conclusion of Williams (2009) and Xu et al. (2021).

We have also identified three other possible regimes of core solidification in which crystallisation can occur concurrently in multiple locations throughout the core (Figs. 3b–d). These three regimes are possible in small planetary cores due to the positive second pressure differential of the liquidus in this region of parameter space, which can result in two intersections of the liquidus and core temperature profiles. While it has not been predicted previously, we are able to identify those regimes because we calculate the temperature and liquidus profiles across the cores, instead of relying on the relative slopes of these quantities. However, improvements in the Fe-FeS phase diagram at low pressures would be beneficial to determine more accurately the conditions under which these intermediate regimes could occur.

The dynamical effect of multiple freezing locations on the evolution of a planetary core is not well explored. Crystallising at both the CMB and at the centre will affect the distribution of latent heat production and light element release on solidification within the core, possibly providing multiple sources of buoyancy fluxes that could drive convection and a dynamo field. Breuer et al. (2015) find that for a super-eutectic Fe-FeS core, crystallisation of FeS solids could first occur in a layer between the CMB and the centre, with the less dense FeS solids then floating upwards towards the CMB and the Fe-enriched fluids sinking downwards. They consider that dynamo generation in this case could be driven by convection caused by the sinking Fe-enriched fluids into the more S-enriched interior, while the solid FeS crystals float passively upwards and do not contribute to the large-scale convective flow within the core (Rückriemen et al., 2015). However, in the regimes we have identified here, crystallisation at the CMB and at the centre could both produce density differences between two fluid phases, which in turn could generate convection and a dynamo. There is therefore a need to quantify the effect of core solidification in multiple locations on the convective power generated during this process.

Additionally, including the full thermochemical evolution of these small planetary cores during solidification could promote simultaneous crystallisation at the CMB and centre. In this study, our method for simulating core cooling and solidification only involves decreasing the core temperature. We have neglected any possible chemical changes in the core fluid during fractional crystallisation, and hence we have neglected the effect of a slowly evolving bulk concentration on the core liquidus. For example, for a core that initially nucleates in the centre but for which the liquidus pressure differential ($\partial T_l/\partial P > 0$) is close to the turning point, e.g. Regime IV (Fig. 3d), expulsion of sulfur from the growing solid inner core will increase the sulfur content of the liquid outer core. This in turn will decrease $\partial T_l/\partial P$, which will eventually become negative and lead to the onset of inward crystallisation as the inner core continues to grow. Similarly, Regime II in which inwards crystallisation starts first before an inner core is also formed could occur across a wider parameter range than suggested here. Such an evolution of the bulk liquid concentration would require any solid iron that formed at the CMB to fall into the core's interior

and remelt, enriching the interior core fluid in iron. This would then increase $\partial T_l/\partial P$ of the liquid inner core and could lead to inner core nucleation. Therefore, including the chemical evolution of the core during crystallisation would likely act to drive these cores rapidly into a state with concurrent inward and outward crystallisation, assuming efficient segregation of the solid and liquid fractions. However, we would not predict this behaviour for asteroid-sized bodies with $P_{CMB} <$ 0.5 GPa as they lie firmly in Regime I regardless of sulfur content, and are therefore predicted to solidify inwardly, regardless of any chemical changes within the core liquid.

Finally, the intermediate pressures from 0.6 GPa to > 2 GPa over which Regimes II–IV operate are unlikely to be relevant for asteroid cores, in which $P_{CMB} <$ 0.5 GPa. These regimes may be relevant for the cores of larger planetary bodies such as the Moon ($P_{CMB} \sim 4-5$ GPa), Ganymede ($P_{CMB} \sim 5-7$ GPa), and Mercury ($P_{CMB} \sim 3$ GPa), especially for high core sulfur concentrations. It would therefore be interesting to extend the pressure range considered here up to these higher pressures for which both the equation of state from Morard et al. (2018) and the liquidus surface from Buono and Walker (2011) are valid, and in particular to investigate the possibility of whether these cores could crystallise simultaneously in more than one location.

4.2. Implications for dynamo activity in asteroid cores

Compositionally driven dynamo activity during inward core solidification must be driven by the sinking of the dense pure iron phase formed below the CMB, in contrast to the geodynamo which is driven by buoyant light-element enriched liquid expelled at the inner core boundary. The mechanism of dynamo generation during inward core solidification has been studied mainly in the context of Jupiter's largest moon, Ganymede, which has an active dynamo field at the present-day (Kivelson et al., 1996, Gurnett et al., 1996, Sarson et al., 1997). The current favoured mechanism is the iron snow model, in which iron crystals form below the CMB, sink into the interior where the adiabat is hotter than the liquidus, and they remelt. This remelting produces a pure iron liquid at shallow depths within Ganymede's core that is denser than the bulk iron–sulfur liquid of the interior. The sinking of this dense iron-rich liquid then produces turbulent convection. This rain-driven convection has been shown by numerical methods (e.g., Christensen, 2015) and by the scaling of analogue experiments to core conditions (e.g., Olson et al., 2017) to produce sufficient entropy to drive Ganymede's observed dynamo field.

However, the small size of asteroid cores (radii of < 300 km) compared to that of Ganymede (radius of ∼ 820 km (Rückriemen et al., 2015)) may prevent remelting of any iron snow that forms. The remelting may be prevented due to the significant undercooling that may be required before the iron alloy liquids can start to crystallise. Recent studies such as Huguet et al. (2018) and Davies et al. (2019) suggest that an undercooling of > 80 K may be required, even at the low pressures of asteroid cores. The magnitude of this undercooling is far greater than the adiabatic temperature between the CMBs and core centres of planetesimals (on the order of a few tens of Kelvin). Therefore the iron crystals would not be expected to remelt in this case as the deep interior of the asteroids' cores would necessarily be colder than the liquidus at all depths due to this undercooling. Lower degrees of supercooling could be possible if nucleation sites are available, but this possibility has not been studied for any sized planetary core.

If the remelting of these iron crystals does not occur, the buoyancy flux required for an iron snow dynamo may not exist in an asteroid core. In the iron snow model, the solid iron crystals themselves are assumed to fall passively through the snow zone at the top of the core and not contribute to powering the dynamo due to their assumed sub-millimetre-scale size (Rückriemen et al., 2015). This assumption of passively falling solids is supported by recent work by Wilczyński et al. (2023) on determining the structure of the F layer above the Earth's inner core. Davies and Pommier (2018) have shown that the entropy provided by the falling solids within a snow zone in the Martian core is negligible until the snow zone is thicker than a few hundred km i.e., greater than the total depth of a planetesimal core. The lack of remelting of the iron snow at depth could also reduce the entropy budget of the core as the latent heat released at the CMB by solidification is no longer reabsorbed at depth.

As such, another mechanism may be required to drive a dynamo in planetesimal cores during top-down solidification. For example, a recent experimental study of the iron snow model has shown that this mode of crystallisation can produce a crystal population with a wide range of sizes (Huguet et al., 2023), which could then interact with the core fluid in a range of different ways from falling passively to stirring up additional flow. It is also possible that the smallest iron particles could dissolve as they fall into the more iron-rich deep interior of the core (Huguet et al., 2018). This could provide a buoyancy flux of liquid iron similar to the iron snow model. Finally, the settling of sediment particles from buoyant plumes into the water column below the plumes has been shown experimentally to drive convection in settings such as estuaries and coastal currents (Hoyal et al., 1999). Therefore, analogue experiments that mimic inward core crystallisation, such as Huguet et al. (2023), may be key to unravelling the physics that the current iron snow models may be missing.

Previous studies of dynamo generation in asteroids have generally focussed on the mechanisms by which unmantled bodies can generate a field, such as Scheinberg et al. (2016) and Neufeld et al. (2019), as they have sought to explain the magnetisation of the rapidly cooled IVA iron meteorites. For example, Neufeld et al. (2019) argues for the periodic delamination of the base of an iron crust at the surface of the IVA parent body, and subsequent dynamo generation driven by stirring of the core fluid as this delaminated layer falls to the centre of the core. These delamination episodes occur approximately every ∼ 30 kyr in an unmantled asteroid. Therefore this mechanism is able to generate a continuous Myr-long magnetic field as the frequency at which the core is stirred up by the falling dendrites is on the same order as the magnetic diffusive timescale within the core. However, given the orders of magnitude slower core cooling rates of the cores of mantled asteroids compared to unmantled ones, the timescales of delamination in a mantled core are likely to be significantly slower and thus the falling crystals may not stir up the core liquid regularly enough to sustain a continuous field.

To summarise, there are difficulties in applying existing models of dynamo generation in inwardly crystallising planetary cores to the cores of most meteorite parent bodies, and thus to interpret the meteorite paleomagnetic record of asteroid core solidification. This is due to their small size in the case of the iron snow model and slow cooling rates in the case of the dendritic delamination models. Therefore, we may require adjustments to these pre-existing models, or an entirely new mechanism for dynamo generation, to explain the late period of magnetic field generation during core crystallisation in meteorite parent bodies from 65 – 250 Myr (Shah et al., 2017, Morard et al., 2018, Bryson et al., 2019a, Maurel et al., 2020, Nichols et al., 2021). Such further work would then enable us to build accurate models of this process for use in constraining the sizes of these extinct planetary bodies.

5. Conclusions

- We predict that the cores of most asteroids crystallise inwardly, regardless of their light element concentration or any uncertainties in the exact value of the core thermal expansivity. This is based on an improved understanding of both the Fe-FeS liquidus surface and the equation of state at low pressures.
- We also show that it may be possible for the cores of larger bodies ($R_c \sim 360 - > 600$ km, depending on sulfur content) to solidify simultaneously at the CMB and centres. This is due to the low

pressure turning point of the Fe-FeS liquidus temperature. However, the relevance of such regimes to any body in our own Solar System is unclear. Further work is required to explore the effect of multiple freezing points on the thermochemical evolution of the core, and subsequent dynamo potential, as well as extending this study to include higher pressures relevant to the Moon, Mercury and Ganymede to test whether any of these bodies could lie in these regimes.

- Dynamo generation during asteroid core solidification must therefore be driven by density differences generated at the core-mantle boundary. However, the iron snow model of dynamo generation is unlikely to apply to asteroid-sized cores due to their minimal adiabatic temperature differences, which prevent the remelting of pure iron crystals as they sink. Instead, a new dynamo mechanism is likely required to explain the period of dynamo generation during asteroid core crystallisation as observed in the meteorite paleomagnetic record across several parent asteroids.

CRediT authorship contribution statement

K.H. Dodds: Writing – original draft, Methodology, Investigation, Formal analysis, Conceptualization. **J.F.J. Bryson:** Writing – review & editing, Supervision, Conceptualization. **J.A. Neufeld:** Writing – review & editing, Supervision. **R.J. Harrison:** Writing – review & editing, Supervision.

Declaration of competing interest

The authors declare that they have no known competing financial interests or personal relationships that could have appeared to influence the work reported in this paper.

Data availability

The numerical data produced in this work can be found in Dodds et al. (2024).

Acknowledgements

We would like to thank two anonymous reviewers for their constructive reviews, as well as Doris Breuer for her editorial handling. This work was funded by UK Natural Environment Research Council grant number NE/L002507/1.

References

Assael, M.J., Kakosimos, K., Banish, R.M., Brillo, J., Egry, I., Brooks, R., Quested, P.N., Mills, K.C., Nagashima, A., Sato, Y., et al., 2006. Reference data for the density and viscosity of liquid aluminum and liquid iron. J. Phys. Chem. Ref. Data 35 (1), 285–300.

Breuer, D., Hauck, S.A., Buske, M., Pauer, M., Spohn, T., 2007. Interior evolution of Mercury. Space Sci. Rev. 132 (2), 229–260.

Breuer, D., Rueckriemen, T., Spohn, T., 2015. Iron snow, crystal floats, and inner-core growth: modes of core solidification and implications for dynamos in terrestrial planets and moons. Prog. Earth Planet. Sci. 2 (1), 39.

Bryson, J.F.J., Neufeld, J.A., Nimmo, F., 2019b. Constraints on asteroid magnetic field evolution and the radii of meteorite parent bodies from thermal modelling. Earth Planet. Sci. Lett. 521, 68–78.

Bryson, J.F.J., Weiss, B., Getzin, B., Abrahams, J., Nimmo, F., Scholl, A., 2019a. Paleomagnetic evidence for a partially differentiated ordinary chondrite parent asteroid. J. Geophys. Res. Planets 124 (7), 1880–1898.

Buono, A.S., Walker, D., 2011. The Fe-rich liquidus in the Fe-FeS system from 1 bar to 10 GPa. Geochim. Cosmochim. Acta 75 (8), 2072–2087.

Chabot, N., Haack, H., 2006. Evolution of asteroidal cores. IIC 7, 1.

Christensen, U.R., 2015. Iron snow dynamo models for Ganymede. Icarus 247, 248–259.

Davies, C.J., Pommier, A., 2018. Iron snow in the Martian core? Earth Planet. Sci. Lett. 481, 189–200.

Davies, C.J., Pozzo, M., Alfè, D., 2019. Assessing the inner core nucleation paradox with atomic-scale simulations. Earth Planet. Sci. Lett. 507, 1–9.

Dodds, K.H., Bryson, J.F., Neufeld, J.A., Harrison, R.J., 2024. Data for dodds et al., The direction of core solidification in asteroids: implications for dynamo generation. http://dx.doi.org/10.5281/zenodo.11657508.

Dorogokupets, P., Dymshits, A., Litasov, K., Sokolova, T., 2017. Thermodynamics and equations of state of iron to 350 GPa and 6000 K. Sci. Rep. 7 (1), 41863.

Driscoll, P., Bercovici, D., 2014. On the thermal and magnetic histories of Earth and Venus: Influences of melting, radioactivity, and conductivity. Phys. Earth Planet. Inter. 236, 36–51.

Elkins-Tanton, L.T., Weiss, B.P., Zuber, M.T., 2011. Chondrites as samples of differentiated planetesimals. Earth Planet. Sci. Lett. 305 (1–2), 1–10.

Goldstein, J., Scott, E., Chabot, N., 2009. Iron meteorites: crystallization, thermal history, parent bodies, and origin. Chem. Erde-Geochem. 69 (4), 293–325.

Gurnett, D., Kurth, W., Roux, A., Bolton, S., Kennel, C., 1996. Evidence for a magnetosphere at Ganymede from plasma-wave observations by the Galileo spacecraft. Nature 384 (6609), 535–537.

Haack, H., Scott, E.R., 1992. Asteroid core crystallization by inward dendritic growth. J. Geophys. Res. Planets 97 (E9), 14727–14734.

Hauck, S.A., Aurnou, J.M., Dombard, A.J., 2006. Sulfur's impact on core evolution and magnetic field generation on Ganymede. J. Geophys. Res. Planets 111 (E9).

Hoyal, D.C., Bursik, M.I., Atkinson, J.F., 1999. Settling-driven convection: A mechanism of sedimentation from stratified fluids. J. Geophys. Res.: Oceans 104 (C4), 7953–7966.

Huguet, L., Le Bars, M., Deguen, R., 2023. A laboratory model for iron snow in planetary cores. Geophys. Res. Lett. 50 (24), e2023GL105697.

Huguet, L., Van Orman, J.A., Hauck, II, S.A., Willard, M.A., 2018. Earth's inner core nucleation paradox. Earth Planet. Sci. Lett. 487, 9–20.

Kanda, M., Hasegawa, N., Itagaki, K., Yazawa, A., 1986. Thermodynamic study of the liquid Fe-S system by use of a drop calorimeter. Thermochimica Acta 109 (1), 275–284.

Kivelson, M., Khurana, K., Russell, C., Walker, R., Warnecke, J., Coroniti, F., Polanskey, C., Southwood, D., Schubert, G., 1996. Discovery of Ganymede's magnetic field by the Galileo spacecraft. Nature 384 (6609), 537–541.

Liu, J., Li, J., 2020. Solidification of lunar core from melting experiments on the Fe–Ni–S system. Earth Planet. Sci. Lett. 530, 115834.

Loper, D.E., 1978. The gravitationally powered dynamo. Geophys. J. Int. 54 (2), 389–404.

Manthilake, G., Chantel, J., Monteux, J., Andrault, D., Bouhifd, M.A., Bolfan Casanova, N., Boulard, E., Guignot, N., King, A., Itié, J.-P., 2019. Thermal conductivity of FeS and its implications for Mercury's long-sustaining magnetic field. J. Geophys. Res. Planets 124 (9), 2359–2368.

Maurel, C., Bryson, J.F., Lyons, R.J., Ball, M.R., Chopdekar, R.V., Scholl, A., Ciesla, F.J., Bottke, W.F., Weiss, B.P., 2020. Meteorite evidence for partial differentiation and protracted accretion of planetesimals. Sci. Adv. 6 (30), eaba1303.

Maurel, C., Bryson, J.F.J., Weiss, B.P., Scholl, A., 2018. Paleomagnetic evidence for a layered partially differentiated iron-meteorite parent body. Lunar Planet. Sci. Conf..

Morard, G., Andrault, D., Antonangeli, D., Bouchet, J., 2014. Properties of iron alloys under the Earth's core conditions. C. R. Geosci. 346 (5–6), 130–139.

Morard, G., Bouchet, J., Rivoldini, A., Antonangeli, D., Roberge, M., Boulard, E., Denoeud, A., Mezouar, M., 2018. Liquid properties in the Fe-FeS system under moderate pressure: tool box to model small planetary cores. Am. Mineral. J. Earth Planet. Mater. 103 (11), 1770–1779.

Morard, G., Sanloup, C., Fiquet, G., Mezouar, M., Rey, N., Poloni, R., Beck, P., 2007. Structure of eutectic Fe-FeS melts to pressures up to 17 GPa: implications for planetary cores. Earth Planet. Sci. Lett. 263 (1–2), 128–139.

Morard, G., Siebert, J., Andrault, D., Guignot, N., Garbarino, G., Guyot, F., Antonangeli, D., 2013. The Earth's core composition from high pressure density measurements of liquid iron alloys. Earth Planet. Sci. Lett. 373, 169–178.

Neufeld, J.A., Bryson, J.F.J., Nimmo, F., 2019. The top-down solidification of iron asteroids driving dynamo evolution. J. Geophys. Res. Planets.

Nichols, C.I., Bryson, J.F., Cottrell, R.D., Fu, R.R., Harrison, R.J., Herrero-Albillos, J., Kronast, F., Tarduno, J.A., Weiss, B.P., 2021. A time-resolved paleomagnetic record of main group pallasites: Evidence for a large-cored, thin-mantled parent body. J. Geophys. Res. Planets 126 (7), e2021JE006900.

Nimmo, F., 2009. Energetics of asteroid dynamos and the role of compositional convection. Geophys. Res. Lett. 36 (10).

Nimmo, F., 2015. Energetics of the core. Treatise Geophys. 8, 27–55.

Olson, P., Landeau, M., Hirsh, B.H., 2017. Laboratory experiments on rain-driven convection: Implications for planetary dynamos. Earth Planet. Sci. Lett. 457, 403–411.

Opeil SJ, C., Consolmagno SJ, G., Safarik, D., Britt, D., 2012. Stony meteorite thermal properties and their relationship with meteorite chemical and physical states. Meteorit. Planet. Sci. 47 (3), 319–329.

Rivoldini, A., Van Hoolst, T., Verhoeven, O., 2009. The interior structure of Mercury and its core sulfur content. Icarus 201 (1), 12–30.

Rückriemen, T., Breuer, D., Spohn, T., 2015. The Fe snow regime in Ganymede's core: A deep-seated dynamo below a stable snow zone. J. Geophys. Res. Planets 120 (6), 1095–1118.

Sarson, G., Jones, C., Zhang, K., Schubert, G., 1997. Magnetoconvection dynamos and the magnetic fields of Io and Ganymede. Science 276 (5315), 1106–1108.

Scheinberg, A., Elkins-Tanton, L., Schubert, G., Bercovici, D., 2016. Core solidification and dynamo evolution in a mantle-stripped planetesimal. J. Geophys. Res. Planets 121 (1), 2–20.
Shah, J., Bates, H.C., Muxworthy, A.R., Hezel, D.C., Russell, S.S., Genge, M.J., 2017. Long-lived magnetism on chondrite parent bodies. Earth Planet. Sci. Lett. 475, 106–118.
Stevenson, D.J., Spohn, T., Schubert, G., 1983. Magnetism and thermal evolution of the terrestrial planets. Icarus 54 (3), 466–489.
Strong, H., Tuft, R., Hanneman, R., 1973. The iron fusion curve and γ-δ-l triple point. Metall. Trans. 4 (11), 2657–2661.
Sun, Y., Zhang, F., Mendelev, M.I., Wentzcovitch, R.M., Ho, K.-M., 2022. Two-step nucleation of the Earth's inner core. Proc. Natl. Acad. Sci. 119 (2), e2113059119.
Weiss, B.P., Tikoo, S.M., 2014. The lunar dynamo. Science 346 (6214), 1246753.
Wilczyński, F., Davies, C.J., Jones, C.A., 2023. A two-phase pure slurry model for planetary cores: one-dimensional solutions and implications for Earth's F-layer. J. Fluid Mech. 976, A5.
Williams, Q., 2009. Bottom-up versus top-down solidification of the cores of small solar system bodies: Constraints on paradoxical cores. Earth Planet. Sci. Lett. 284 (3–4), 564–569.
Wilson, A.J., Alfè, D., Walker, A.M., Davies, C.J., 2023. Can homogeneous nucleation resolve the inner core nucleation paradox? Earth Planet. Sci. Lett. 614, 118176.
Xu, F., Morard, G., Guignot, N., Rivoldini, A., Manthilake, G., Chantel, J., Xie, L., Yoneda, A., King, A., Boulard, E., et al., 2021. Thermal expansion of liquid Fe-S alloy at high pressure. Earth Planet. Sci. Lett. 563, 116884.